Materials Today Physics 6 (2018) 53–59

Contents lists available at ScienceDirect

Materials Today Physics

journal homepage: https://www.journals.elsevier.com/materials-today-physics

Thermal boundary resistance correlated with strain energy in individual Si film-wafer twist boundaries

D. Xu [a], R. Hanus [b], Y. Xiao [a], S. Wang [a], G.J. Snyder [b], Q. Hao [a, *]

[a] Department of Aerospace and Mechanical Engineering, University of Arizona, Tucson, AZ 85721, USA
[b] Department of Materials Science and Engineering, Northwestern University, Evanston, IL 60208, USA

ARTICLE INFO

Article history:
Received 22 July 2018
Received in revised form
25 August 2018
Accepted 31 August 2018
Available online 5 October 2018

Keywords:
Thermal boundary resistance
Strain energy
Twist grain boundary
Hot press
Phonon

ABSTRACT

Nanoscale interfaces, such as grain boundaries (GBs) within a polycrystalline material, play an important role in suppressing the phonon heat transport. The interfacial thermal resistance R_K of a GB has a strong dependence on the detailed interfacial atomic structure, including the misorientation between two grains and GB dislocations. Along this line, numerous molecular dynamics simulations on R_K have been carried out on a twist Si GB. Owing to the challenge of measuring such a GB within a bulk material, these simulations are rarely compared with experimental data. In this work, a super-flexible 70-nm-thick Si thin film was hot pressed onto a Si wafer to represent a twist GB. The R_K of the film-wafer interface was measured as a function of the rotation angle between the film and the wafer. The experimental data were further compared with an analytical model to interpret the twist angle dependence of the measured R_K. It was found that the strain part of the grain-boundary energy is correlated with the measured twist-angle-dependent R_K.

1. Introduction

A grain boundary (GB) inside polycrystalline materials can transmit or reflect incident phonons. Such interfacial phonon scattering introduces an interfacial thermal resistance R_K, known as the Kapitza resistance [1,2]. With a high volumetric density of GBs, phonon transport within a material with fine grains can be largely suppressed by GBs [3]. The reduction of lattice thermal conductivity k_L by GBs has been exploited to develop better thermal insulation and thermoelectric materials [4]. In addition, the R_K for GBs and other interfaces can significantly impede heat spreading in electronic devices, thus creating challenges for thermal management [3,4].

In a polycrystal, various GBs with different structure and energies are present simultaneously, which can be described through the GB character distribution [5]. GBs within this distribution have varying crystal misorientations (with five macroscopic degrees of freedom) and varying atomic structures at the interface (additional microscopic and atomic degrees of freedom). The total GB energy (γ_{GB}) is given as $\gamma_{GB} = \gamma_{core} + \gamma_{strain}$, where γ_{core} and γ_{strain} are the energy due to broken bonds across the interface and the energy due to GB strain fields, respectively. The atomic structure of many GBs in their low total energy atomic configuration minimizes the number of broken bonds across the interface and is viewed as arrays of GB dislocations separated by strained perfect crystal [5]. In contrast, GBs described as disordered or amorphous tend to contain larger amounts of broken bonds across the interface and, while they usually have low amounts of strain energy, they tend to be higher in total energy [6]. It is widely accepted that the structure of a GB can influence phonon transport across it [3,4]. However, detailed studies are required to determine which attributes of this GB structure and energy are the most important for phonon transport.

In some molecular dynamics (MD) studies, the total GB energy (γ_{GB}) is proposed to be associated with R_K [7–9]. Additionally, the local strain field that forms at a GB has been shown to affect the phonon transport [10]. In the widely used acoustic mismatch model (AMM) and diffuse mismatch model (DMM), however, the complexity associated with the structure and energy of a GB is usually neglected. Assuming specular phonon scattering on an interface, the AMM fails to predict the GB R_K because of the same acoustic impedance between two grains made of the same material [3]. Developed for a rough interface with diffusive phonon scattering, the DMM [2] instead predicts a fixed GB phonon transmissivity τ_{GB} of 0.5 at all frequencies due to structure symmetry of a GB [11]. Because high-frequency phonons are anticipated to be

* Corresponding author.
E-mail address: qinghao@email.arizona.edu (Q. Hao).

https://doi.org/10.1016/j.mtphys.2018.08.002
2542-5293/

scattered stronger by a GB, τ_{GB} should decrease with an increased phonon frequency, and the DMM is thus expected to be over-simplified [8,12,13]. More advanced MD simulations have been carried out to predict the R_K for various GBs [8,14–17]. However, experimental measurements are often lacking to validate these predictions, mainly due to the challenge in measuring a single GB within a three-dimensional bulk material [4]. In most data analysis, the averaged R_K of all GBs within a polycrystalline material can be extracted using an effective medium formulation, whereas the difference between varied GBs is neglected [18–22].

Due to the challenge in measuring a single GB within a bulk material, bonding between identical wafers with relative rotation has been used to gain insights into the phonon transport across twisted GBs [23,24]. In these studies, two identical crystals are rotated relatively around an axis that is perpendicular to the GB plane. A phonon focusing image has also been taken for twist-bonded wafers [25]. A major challenge for such studies is maintaining high-quality bonding across the whole wafer. This requires both wafers to be atomically flat to avoid the creation of voids or unintended structural defects. From this perspective, much better thermal bonding can be achieved using super-flexible thin films as one of the crystals. This is essentially due to a large initial film-wafer contact area and negligible separation or fracture during the bonding process. Even for a film and a wafer with a large lattice mismatch and/or a large twist angle, a high-quality interface can still be obtained, which is challenging when bonding two rigid wafers. For device fabrication, extremely high-quality bonding has been demonstrated between a 200-nm-thick and millimeter-sized Si membrane and a Ge wafer [26]. High-resolution transmission electron microscopy (TEM) shows a thin ~1 nm region for the bonded Si-Ge interface. With moderate pressure at 473 K, stacked nanometer thick membranes can be used to form a Si-Ge- superlattice with a cross-plane k_L below 2 W/m·K [27]. For phonon transport studies, these high-quality interfaces for film-wafer or film-film bonding provide ideal model systems for real GBs that are formed by hot pressing nanopowder into a bulk material [28,29].

In this work, thermal investigation of twist GBs was performed with a 70-nm-thick (100) Si thin film hot pressed onto a (100) Si wafer. The high-quality interfaces achieved via film-wafer bonding was confirmed by TEM studies and enabled thermal studies of GBs across a large range of misorientation angles. Temperature-dependent interfacial R_K between the film and the wafer was carried out for different twist angles between the film and the wafer. GBs with a low (<15°) and high twist angle were measured, which was enabled by the film-wafer bonding. This broad range of twist angles reached beyond previous studies, which used wafer-wafer bonding methods and were constrained to small twist angles [23,24]. Detailed electron microscopy studies were carried out on representative samples to reveal the interfacial atomic structures. An analytical model based on such an interfacial structure was used to interpret the observed twist-angle dependence of R_K. Although some earlier studies associated R_K with the total GB energy γ_{GB} [7–9], this work suggests a correlation between R_K and the strain-part of the GB energy, γ_{st}. Our results provide new insights into phonon transport across GBs, which are important for technologies ranging from microelectronics to energy materials.

2. Material and methods

2.1. Sample preparation

The (100) thin films used were released from a commercial silicon-on-insulator (SOI) wafer and transferred onto another (100) Si wafer with 500 μm thickness. The film transfer was performed in diluted hydrogen fluoride (HF) acid to prevent oxidation of Si, which was found on the bonded interface of Si wafers [24] and at GBs within hot-pressed nanocrystalline silicon [12]. The whole transfer process followed that used for graphene, with a photoresist layer to protect the film during the transfer process [30]. This photoresist layer was later dissolved in acetone. Before the hot press, the film was further annealed at 473 K to ensure good sample-substrate contact. A thin SiO_2 layer with 20 nm thickness was then deposited onto the sample to avoid possible contamination during the following hot press. The hot press was then carried out under N_2 protection at around 1223 K with 1-min holding. The rapid heating was provided by an induction heater, as used for bulk-material synthesis [31]. Roughly 50 MPa pressure was applied with a graphite die and this pressure was uniformly distributed across the film using a soft graphite foil. After the hot press, the SiO_2 layer was etched off by HF. The residual graphite was removed together with the SiO_2 layer, as shown in Fig. 1a.

The employed hot-press condition should be compared with that used for nanocrystalline bulk Si, where a higher hot-press temperature (1327–1523 K) with 0–2.5 min holding was required to obtain up to 99.5% theoretical density [12]. For bulk materials, this higher hot-press temperature is required to soften the irregular-shaped nanopowder for better compaction. For film-wafer bonding, a lower bonding temperature was usually used because the film and wafer were in good contact already. In practice, further increasing the hot-press temperature may cause cracks on the film when the twist angle between the film and the wafer was large. To further improve the bonding quality, all samples were finally sealed in a vacuum tube and annealed at 1173 K for 1 hr. The interfacial R_K for all samples was measured after annealing, and selected samples were also measured right after the hot press.

Cross-sectional TEM studies were also carried out on representative samples with a low to a high film-wafer twist angle (Fig. 1b and c). GB regions with around 3.0 nm and 4.25 nm thicknesses were observed in the TEM images of samples with 3.4° and 86.5° twist angles, respectively. Interfacial layers were observed with no apparent structure (appears amorphous) when viewed in this direction, as suggested by MD simulations previously [32]. Some GB structures were found later within this “amorphous” region [33]. These interfacial layers were thicker than the ~1 nm interfacial layer for the previous bonding between a Si film and a Ge wafer [26], which was performed only at 673 K for 30 min. For all samples, further checking with energy-dispersive X-ray spectroscopy suggested almost uniform surface natural oxidation across the entire cross section, i.e. there is no amorphous SiO_2 layer at the film-wafer interface. In previous thermal studies using wafer-wafer bonding, an extra SiO_2 layer was found on the bonded interface so that the measured R_K did not represent that for a “clean” GB in bulk materials [24]. This oxide layer was prevented in this study with careful oxygen protection during the hot press.

To better understand the GB region, TEM images normal to the GB plane (i.e. plane view) were also taken to reveal that the interfacial region is not amorphous but shows a periodic GB dislocation structure for the sample with a 3.4° twist angle (Fig. 1d and e). This further confirms that clean interfaces with low-energy atomic configurations were synthesized. In the literature, similar TEM studies were carried out for the bonding between the device layer of a SOI wafer and a Si wafer [34]. A similar dislocation network was observed in this earlier study. However, the device layer was not released from the SOI wafer during the thermal bonding, which differs from the current work.

2.2. Offset 3ω measurement

The obtained film-on-substrate structure was measured with an offset 3ω method [35] by comparing the measurements in regions

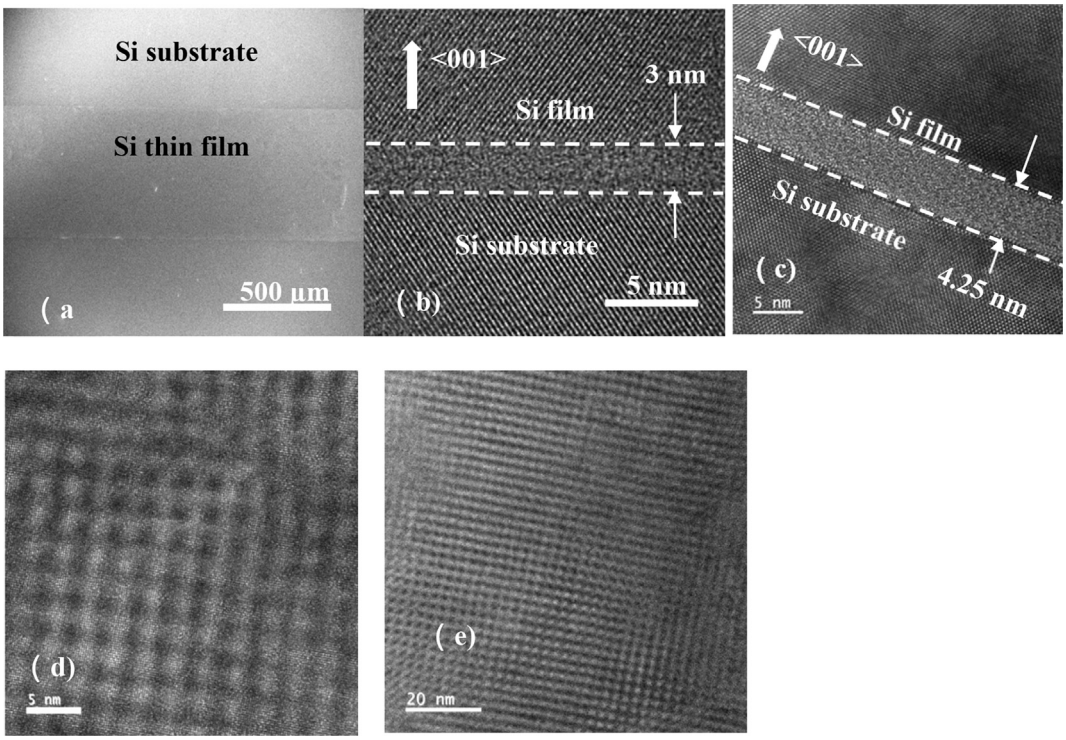

Fig. 1. (a) The top-view scanning electron microscopy (SEM) image of a 70-nm-thick Si film bonded onto a Si substrate by hot press. Cross-sectional TEM images of film-wafer interfaces for a twist angle of (b) 3.4° and (c) 86.5° after 1173 K anneal. The GB region is enclosed by dashed lines, with the thickness indicated. Plane-view TEM image for the GB with a 3.4° twist angle, with (d) high and (e) low magnifications. TEM, transmission electron microscopy; SEM, scanning electron microscopy; GB, grain boundary.

with and without the bonded Si film. In such measurements, an AC current with an angular frequency ω was passed through a metal-line heater/thermometer, and the 3ω voltage signal was sensed to extract the thermal properties of the underlying structure. Similar comparison measurements were carried out on a-Si:H thin films grown on a MgO substrate [36]. To avoid current leakage, the wafer-film assembly was uniformly coated with a 20-nm-thick amorphous SiO_2 layer for electrical insulation. The thickness of the SiO_2 coating on and off the Si-film-cover region was checked with spectroscopic reflectometry (Filmetrics F-20), and the thickness variation was within 0.5 nm in general, ensuring good accuracy for comparison measurements. A 20-μm-wide and millimeter-long Cr/Au line was then deposited as the thermometer/heater used for 3ω measurements. The Au layer and its underlying Cr adhesion layer were 200 and 10 nm thick, respectively. In thermal analysis, the width of the metal line was much larger than the 70 nm film thickness so that one-dimensional heat conduction across the film thickness can be assumed. As the reference, an identical metal line was also patterned on the same wafer and near the Si film.

In Fig. 2, the two comparison measurements have the in-phase AC temperature oscillation ΔT_{AC} at all frequencies shifted by a constant value, i.e. $P(R_{Film} + R_K)/A$. Here, P, A, and R_{Film} are the amplitude of the heating power at the 2ω frequency, area of the metal line, and the cross-plane thermal resistance of the film, respectively. Both R_{Film} and R_K are evaluated per unit area of the thin film. In Fig. 2, the shift of $\Delta T_{AC}A/P$ is thus determined by $R_{Film} + R_K$ and is unrelated to the selected P value. The slope of all curves yields the thermal conductivity of the Si wafer. The room-temperature k value is measured as 135–142 W/m·K, which is within 10% divergence from $k = 150$ W/m·K for bulk Si. The linear regime is obtained when the thermal penetration depth is at least 2.5 times larger than the metal-line width [37] as 20 μm here. With the thermal diffusivity $\alpha \approx 8 \times 10^{-5}\ m^2/s$ for the Si substrate at

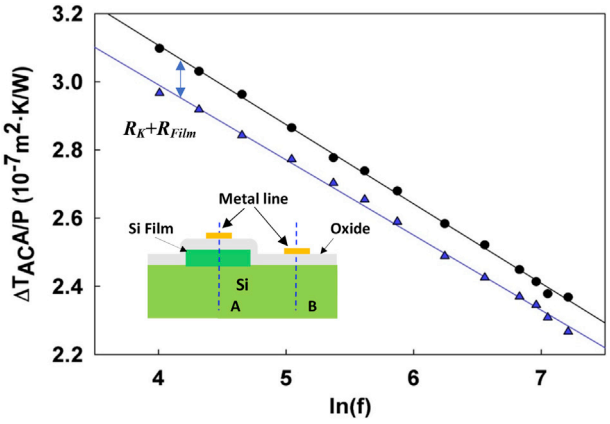

Fig. 2. $\Delta T_{AC}A/P$ for a typical comparison 3ω tests, with the inset showing the cross-section diagram of the measurement setup. The symbols are measurement results, and the curves are linear fitting. The black curve and circles are for location A, with SiO_2-coated film-wafer assembly. The blue curve and triangles are for location B, without the Si film. (For interpretation of the references to color in this figure legend, the reader is referred to the Web version of this article.)

300 K, the penetration depth is computed as $\sqrt{\alpha/2\omega}$. At 300 K, the employed AC frequency $f = \omega/2\pi$ should be less than 2.5 kHz. In all measurements here, the maximum f is about 1 kHz in general. This frequency range is also suitable for measurements below 300 K, with larger α values and thus a higher thermal penetration depth.

2.3. Uncertainty of offset 3ω measurement

In previous 3ω studies, uncertainty analysis emphasized the error in the dR_{Metal}/dT slope for the measured electrical resistance

R_{Metal} of metal lines. In data analysis, dR_{Metal}/dT was used to convert the measured AC voltages into ΔT_{AC} [38,39]. This error was mainly due to the 1–2 K accuracy (offset) of thermocouple reading in temperature-dependent measurements. However, this error may be overestimated because the slope dR_{Metal}/dT should be mostly affected by the ~0.01 K repeatability of thermocouple reading [40]. Along this line, highly accurate Seebeck coefficients can be obtained from the slope $d\Delta V/d\Delta T$ for varied voltage difference ΔV and temperature difference ΔT of a few Kelvins applied across a sample [41].

In this study, aforementioned dR_{Metal}/dT error is neglected. For all metal lines, $R^2 > 0.9999$ is obtained for the linear fitting of $R_{Metal}(T)$ over 77–300 K, indicating highly reliable dR_{Metal}/dT values. In this situation, the uncertainty of measured $R_{Film} + R_K$ mostly results from the electrical measurements and the possible thickness variation of the SiO_2 coating at locations A and B in Fig. 2.

In all measurements, $\Delta T_{AC}A/P$ is averaged over all frequencies in Fig. 2 to extract $R_{Film} + R_K$. For this averaged $R_{Film} + R_K$, the half width of its 95% confidence interval (u_R) ranges from 1.2×10^{-10} to 3×10^{-9} m^2 K/W for all temperature-dependent measurements. This corresponds to less than 8% divergence from the extracted $R_{Film} + R_K$ value.

The accuracy of the offset 3ω measurements is first calibrated by measuring the cross-plane thermal conductivity of amorphous SiO_2 layers deposited onto a Si wafer by electron beam evaporation. Similar measurements have been carried out before to validate the offset method [36,42]. Fig. 3a shows $\Delta T_{AC}A/P$ for measurements with different SiO_2 thicknesses. In reference, a dashed line is also added as ΔT_{AC} for the case without any oxide coating, which is predicted by the theoretical model [35]. Fig. 3b plots the extracted $R_{Film} + R_K$ as a function of film thickness t. Because the thermal conductivity k of amorphous SiO_2 is weakly dependent on the film thickness, the slope of the curve is thus $1/k$. The linear fitting of measured data yields room-temperature $k \approx 0.8$ W/m·K for SiO_2, which is within the 0.618–0.947 W/m·K range reported before [43]. This value is lower than bulk value as 1.4 W/m·K and is attributed to defects within electron-beam deposited SiO_2. With this k value, the aforementioned 0.5 nm variation in the thickness of deposited SiO_2 corresponds to $u_{SiO_2} = 6 \times 10^{-10}$ K m^2/W as the uncertainty for extracted $R_{Film} + R_K$ due to oxide coating. To further check the influence of the selected electrical insulation layer, a few real film-wafer assemblies were also re-measured by replacing the original SiO_2 layer with a 30-nm-thick Al_2O_3 layer. Still by comparing measurements at locations A and B in Fig. 2, the subtracted $R_{Film} + R_K$ for the film-wafer bonding diverged from that measured with SiO_2 coating by less than 8×10^{-10} m^2K/W at 300 K.

2.4. Cross-plane R_{Film} calculation

The offset 3ω method only yielded the summation $R_{Film} + R_K$. To extract R_K, the cross-plane thermal resistance of the film R_{Film} should be known first. In a similar study on bonded Al_2O_3 wafers, R_{Film} was simply neglected. R_{Film} in this early study would be the resistance of the 1–2 μm-thick Al_2O_3 film that was polished down from a top wafer bonded to the bottom wafer [23]. This led to overestimated R_K. In our study, R_{Film} was always subtracted from the measured $R_{Film} + R_K$ to provide more reliable R_K values.

Because direct thermal measurements were challenging for ultra-thin films, the cross-plane thermal conductivity k of a thin film and thus $R_{Film} = t/k$ were estimated using the bulk phonon mean free paths (MFPs) and a film thickness of $t = 70$ nm. Only three acoustic branches were considered due to the weak contribution by optical branches. For a film surface roughness as small as 1.63 nm, complete diffusive phonon scattering by film boundaries has been suggested above 100 K [44]. Therefore, complete diffusive phonon scattering by the film boundary was assumed in all calculations. Because phonon phase coherence was mostly destroyed by diffusive phonon scattering, no phonon wave effects were considered here, which also resulted from the large film thickness in comparison with the dominant phonon wavelengths, i.e. a few nanometers for the investigated temperature range [45].

In modeling, both k and R_K may depend on the film thickness t and interfacial phonon scattering. In detailed phonon transport analysis, R_K is affected by the energy distribution of phonons incident on the interface. Under strong ballistic phonon transport across an ultra-thin film, phonon temperature within the thin film is almost uniform so that the incident phonons originate from locations with very close temperatures. In this situation, the film thickness dependence of R_K can be very weak [46]. When this one-dimensional phonon transport analysis is extended to three-dimensional polycrystalline materials, phonon transport modeling still considers phonon size effects within each grain and R_K between adjacent grains [18,47]. The extracted R_K for film-wafer interfaces can thus be viewed as R_K for GBs associated with grain sizes that are much smaller than majority phonon MFPs. Based on first-principles calculations, around 50% of the room-temperature k_L is contributed by phonons with MFPs longer than 1 μm [48]. With weak phonon scattering, the contribution from long-MFP phonons monotonously increases at decreased temperatures. Therefore, the extracted R_K can be generally accurate for grain sizes of a few hundred nanometers or less.

Based on the kinetic theory, the cross-plane lattice thermal conductivity $k \approx k_L$ is given as

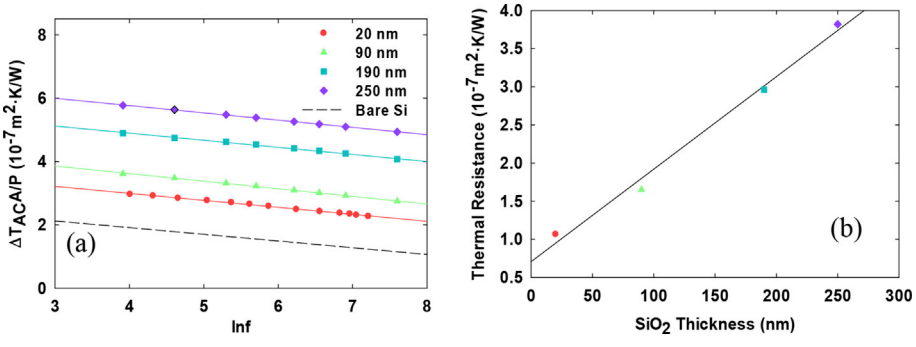

Fig. 3. (a) $\Delta T_{AC}A/P$ for measured amorphous SiO_2 layers, with the dashed line as the computed result for bare Si. (b) Thermal resistance of SiO_2 films as a function of the film thickness. This thermal resistance contains the cross-plane R_{Film} for the SiO_2 layer, and R_K (y-intercept value) for SiO_2/Si and metal/SiO_2 interfaces.

$$k_L = \frac{1}{3}\sum_{i=1}^{3}\int_0^{\omega_{max,i}} C_i(\omega)v_{g,i}(\omega)\Lambda_i(\omega)d\omega, \quad (1)$$

where the subscript i indicates the phonon branch, ω is the phonon angular frequency, C is the differential phonon specific heat per unit volume, v_g is the phonon group velocity, and Λ is the phonon MFP. Assuming diffusive film-boundary phonon scattering, the phonon MFP $\Lambda_i(\omega)$ is modified from the bulk value $\Lambda_{Bulk,i}(\omega)$ by the film thickness t, given by Majumdar as [49].

$$1/\Lambda_i(\omega) = 1/\Lambda_{Bulk,i}(\omega) + 4/3t. \quad (2)$$

The same MFP modification can be found for gas molecules confined within a gap of size t [50], again as classical size effects. More accurate calculations have been proposed using the lattice Boltzmann method [51] but Eq. (2) is still used in this work for simplicity. Detailed phonon transport analysis for film-on-substrate structures can also be found elsewhere [46,52].

Using first-principles phonon MFPs computed by Esfarjani et al. [48], the room-temperature k_L can be predicted as a function of the film thickness (solid line in Fig. 4a). These phonon MFPs are validated by experiments on bulk Si [53]. In data analysis, available k measurements on nanowires [54,55] and nanoporous Si films [56] can both be well explained using these phonon MFPs. The first-principles prediction also agrees well with a separated calculation using the exact phonon dispersion and fitted phonon MFPs [57] (dashed line in Fig. 4a). Both predictions are higher than the experimental data on a suspended 500-nm-thick Si film [58] (filled circle in Fig. 4a). The divergence has been attributed to the defects in real samples and some uncertainties in time-domain thermoreflectance measurements [57]. The measurement data [58] can be an underestimate because the same work also reports nanoporous Si films with k values much lower than theoretical predictions [59].

Below 300 K, detailed temperature dependence is not given for the first-principles phonon MFPs [48]. In another work, Ward and Broido suggest $\Lambda_{Bulk,i}(\omega,T) \sim 1/g(T)$ for all acoustic phonons [60]. This simple temperature dependence is employed here to estimate temperature-dependent bulk phonon MFPs based on room-temperature phonon MFPs. The temperature-related function is

$$g(T) = T[1 - \exp(-3T/\Theta_D)], \quad (3)$$

where the Debye temperature is $\Theta_D = 645$ K for Si [60]. Using Eq. (3), temperature-dependent k_L along the cross-plane direction is computed and presented in Fig. 4b. These values are used to calculate R_{Film} in the data analysis.

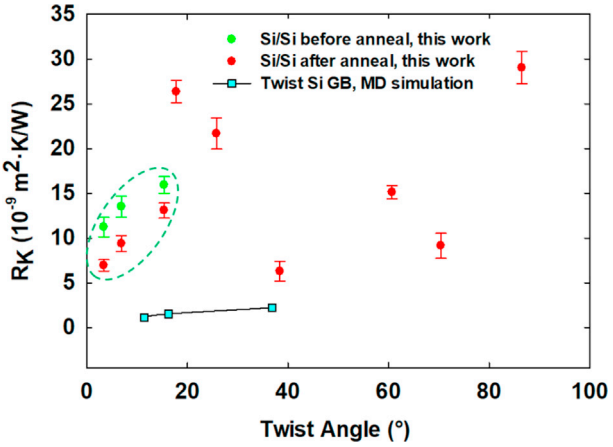

Fig. 5. Comparison between measured and predicted R_K values of twist GBs at 300 K. Samples enclosed by the dashed line are measured both before and after the anneal. MD, molecular dynamics; GB, grain boundary.

3. Results

3.1. Measured twist-angle-dependent R_K

In Fig. 5, the extracted room-temperature R_K values are plotted as a function of the twist angle between the film and the wafer. The error bars assume the overall uncertainty as $\sqrt{u_R^2 + u_{SiO_2}^2}$, where both u_R and u_{SiO_2} are discussed earlier. Three low-twist-angle samples were measured before (green circle) and after (red circle) the 1173 K annealing. All measured R_K values are higher than predictions by MD simulations (square) for a twist (100) Si GB [8]. Other MD simulations can also be found in an earlier study [13]. However, the employed atomic structures on a GB are usually oversimplified when compared with that revealed in the TEM images, particularly for the strained interfacial layer with an array of dislocations. In addition, these MD simulations apply the Si Stillinger-Weber interatomic potential which is known to underestimate Grüneisen parameters, particularly for transverse phonons (see Table I of Porter et al. [61]). Since phonons scatter off strain fields through anharmonic terms in the interatomic potential, underestimation of the Grüneisen parameters should underestimate R_K if phonon-strain effects are important.

Representative samples after annealing are also measured for temperature-dependent R_K that monotonically decreases at increased temperatures (Fig. 6). This trend is consistent with MD studies on twist (100) Si GBs [8] though the measured R_K values are much higher than MD predictions, presumably due to the underestimated phonon-strain field interaction. Part of this trend is

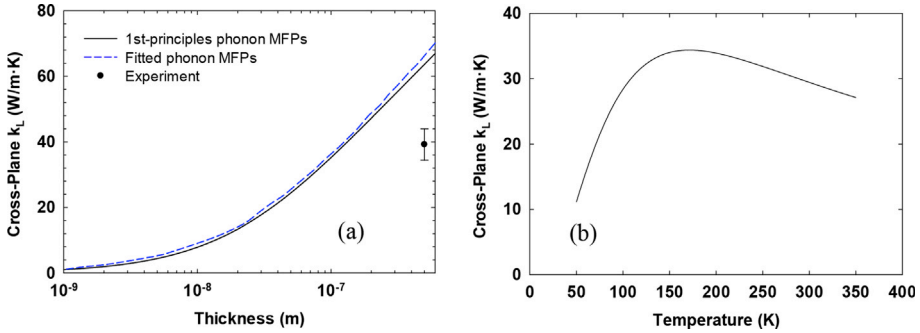

Fig. 4. (a) Cross-plane k_L as a function of the film thickness at 300 K. The solid and dashed lines are predictions using first-principles phonon MFPs and fitted phonon MFPs, respectively. The solid circle is the experimental data by Hopkins et al. [58]. (b) Temperature-dependent cross-plane k_L computed for a 70-nm-thick Si film.

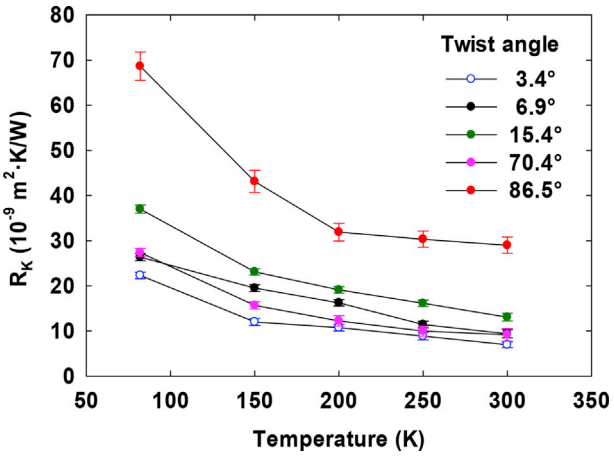

Fig. 6. Temperature-dependent R_K for representative samples.

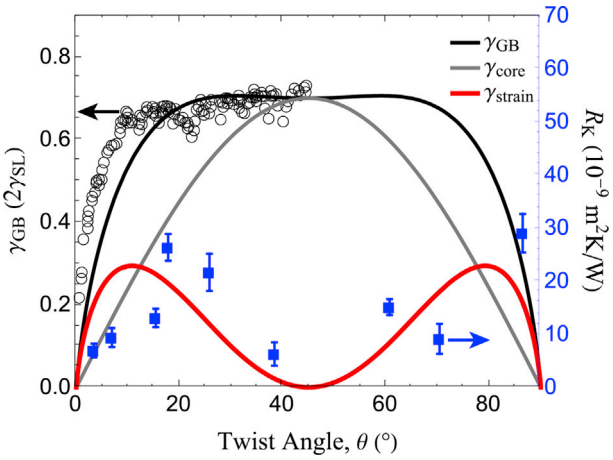

Fig. 7. Experimental data of the GB energy (γ_{GB}) and thermal boundary resistance (R_K) of Si twist GBs. Open circles (left axis) are data from Otsuki [63]. Blue squares (right axis) are data from this study for samples after annealing. The lines are associated with the left axis and show the extended Read-Shockley model for GB energies, where the core energy (γ_{core}) and the strain energy (γ_{strain}) sum to give γ_{GB}. (For interpretation of the references to color in this figure legend, the reader is referred to the Web version of this article.)

attributed to more activated phonon modes at elevated temperatures to enhance the heat transfer across a GB.

3.2. Extended Read-Shockley model for GB energies

Although GBs are varied and complex, GB energy γ_{GB} is a useful single parameter that correlates with many properties. The widely used Read-Shockley model [62] effectively describes [6,7] the structure of a GB as an array of dislocations, as shown in Fig. 1d. In general, γ_{GB} is split into two parts, i.e. the core energy γ_{core} and the strain energy γ_{strain}. The Read-Shockley model was generalized by Wolf [6] into what is now called the *extended* Read-Shockley model, where the core energy response due to broken bonds across the interface (E_c/b) and the GB strain energy response (E_{st}/b) are treated as fitting parameters:

$$\gamma_{GB} = \gamma_{strain} + \gamma_{core} = 2\sin 2\theta\left[\frac{E_c}{b} - \frac{E_{st}}{b}\ln(\sin 2\theta)\right], \text{ with } 0^\circ \le \theta \le 90^\circ \quad (4)$$

where θ is the GB twist angle.

We now apply this model to experimental data of γ_{GB} for (100) Si twist boundaries provided by Otsuki [63]. This early study on Si-Si bicrystals was made using a solid-state bonding method at 1473 K for 10 hr. The boundary was wetted with a liquid Sn-Al alloy at 1473 K for three days in Ar. Grooves were formed on the surface at the GB to satisfy the energy balance between the GB energy (γ_{GB}) and the solid-liquid interfacial energy (γ_{SL}). The dihedral angle of the groove is thus a measure of γ_{GB} normalized by $2\gamma_{SL}$, which is taken to be a constant. In a more recent study, the GB energy γ_{GB} was associated with the twist angle θ between a film and its bonded wafer [26]. A comparison of the GB energy model in Eq. (4) to the experimental data is shown in Fig. 7 with $E_c/b = 0.35\,(2\gamma_{SL})$ and $E_{st}/b = 0.4\,(2\gamma_{SL})$. As θ increases, the spacing between GB dislocations decreases. As can be seen in Fig. 7, γ_{strain} peaks between $\theta = 10$ and 15° and decreases at higher θ due to interaction between individual GB dislocations.

Watanabe et al. have analyzed the thermal boundary resistance data of diamond obtained via MD simulations [7]. They concluded that the Kapitza length, which is directly proportional to R_K, is correlated with the γ_{GB}. In MD studies of two-dimensional polycrystalline graphene [9] or a twist Si GB [8], a larger γ_{GB} was also found to lead to a higher R_K. Comparing our experimental data of R_K of annealed Si twist GBs to the extended Read-Shockley model, it seems that R_K may be correlated with γ_{strain}, the interfacial strain energy of the twist GB (Fig. 7), instead of the total energy γ_{GB}. To accurately capture the phonon-strain-field interaction in a MD simulation, the anharmonicity and Grüneissen parameters of the material need to be accurately represented by the interatomic potential employed. Because the transverse Grüneissen parameters of the Stillinger-Weber and Tersoff potentials are significantly underestimated, the correlation between R_K and γ_{st} may be missed in existing MD simulations [61].

We note that this GB energy model neglects energy cusps that occur at special GBs, i.e. the Σ3 boundary at $\theta = 36.9°$, and the non-zero γ_{GB} at $\theta = 90°$. While the measured γ_{GB} does indeed show cusps in GB energy at special boundaries, the experimental data available show that they are relatively shallow. Although there will be additional complexities and variations from this model when special boundaries are considered, we argue that the general trend of GB energy captured by the extended Read-Shockley model may hold.

4. Discussion

In this work, bonding between a 70-nm-thick (100) Si thin film and a (100) Si wafer is used to prepare twist GBs for phonon transport studies. The bonding formation is under comparable conditions as the hot press for bulk materials. This allows detailed studies of individual GBs with controllable misorientations, particularly for GBs with a high twist angle. In contrast, existing measurements of varied bulk nanocrystalline Si only extract the averaged influence of many GBs on phonon transport [12,18]. Directly measuring a single GB inside a bulk polycrystalline material still remains as a challenge.

Although existing studies often suggest a strong correlation between the total GB energy γ_{GB} and R_K [7–9], the twist angle dependence of our measured data instead indicates strong influence on R_K from the strain component of the GB energy γ_{strain}. This finding indicates that the nanometer-thick strained interfacial layer can be critical to the phonon transmissivity and its temperature dependence. We suspect that strain field effects on R_K should be important for general hetero-interfaces as well [64]. Along this line, more attention should be paid to the role of a strained layer in the

interfacial phonon transport, which is critical when engineering phonon transport across interfaces [65–68].

Acknowledgments

Hao thanks the support from National Science Foundation CAREER Award (grant number CBET-1651840). Dongchao thanks the help from Bo Xiao for the measurements. The authors also thank Dr. Lingping Zeng for providing first-principles phonon MFPs. Hanus acknowledges support from the Johannes and Julia Randall Weertman Graduate Fellowship.

References

[1] P.L. Kapitza, J. Phys. (Moscow) 4 (1941) 181.
[2] E.T. Swartz, R.O. Pohl, Rev. Mod. Phys. 61 (3) (1989) 605.
[3] D.G. Cahill, et al., J. Appl. Phys. 93 (2) (2003) 793.
[4] D.G. Cahill, et al., Appl. Phys. Rev. 1 (1) (2014) 011305.
[5] L. Priester, Grain Boundaries: from Theory to Engineering, Springer Science & Business Media, 2012.
[6] D. Wolf, Structure and energy of grain boundaries, in: Handbook of Materials Modeling, Springer, 2005, p. 1953.
[7] T. Watanabe, et al., J. Appl. Phys. 102 (6) (2007) 063503.
[8] S.-H. Ju, X.-G. Liang, J. Appl. Phys. 113 (5) (2013) 053513.
[9] H. Liu, et al., J. Phys. Chem. C 118 (42) (2014) 24797.
[10] S. Shekhar, A.H. King, Acta Mater. 56 (19) (2008) 5728.
[11] Q. Hao, et al., Appl. Phys. Lett. 97 (6) (2010) 063109.
[12] Z. Wang, et al., Nano Lett. 11 (6) (2011) 2206.
[13] P. Schelling, et al., J. Appl. Phys. 95 (11) (2004) 6082.
[14] A. Maiti, et al., Solid State Commun. 102 (7) (1997) 517.
[15] W. Pickett, et al., Model. Simulat. Mater. Sci. Eng. 4 (4) (1996) 409.
[16] C. Kimmer, et al., Phys. Rev. B 75 (14) (2007) 144105.
[17] W.K. Kim, et al., Int. J. Heat Mass Tran. 100 (2016) 243.
[18] Q. Hao, J. Appl. Phys. 111 (1) (2012) 014307.
[19] H.-S. Yang, et al., Acta Mater. 50 (9) (2002) 2309.
[20] C.-W. Nan, R. Birringer, Phys. Rev. B 57 (14) (1998) 8264.
[21] H. Dong, et al., Sci. Rep. 4 (2014) 7037.
[22] J. Anaya, et al., Acta Mater. 139 (2017) 215.
[23] K. Tai, et al., Appl. Phys. Lett. 102 (3) (2013) 034101.
[24] D.H. Hurley, et al., J. Appl. Phys. 109 (8) (2011) 083504.
[25] M. Msall, et al., Phys. Rev. Lett. 85 (3) (2000) 598.
[26] A.M. Kiefer, et al., ACS Nano 5 (2) (2011) 1179.
[27] D. Grimm, et al., Nano Lett. 14 (5) (2014) 2387.
[28] B. Poudel, et al., Science 320 (5876) (2008) 634.
[29] A.J. Minnich, et al., Energy Environ. Sci. 2 (5) (2009) 466.
[30] Y. Chen, et al., Adv. Sci. 3 (8) (2016).
[31] A.D. LaLonde, et al., Rev. Sci. Instrum. 82 (2) (2011) 025104.
[32] J.K. Bohrer, et al., AIP Adv. 7 (4) (2017) 045105.
[33] Private Communication with Prof. Dietrich Wolf for their published MD simulation in Ref. 32.
[34] J. Rouviere, et al., Appl. Phys. Lett. 77 (8) (2000) 1135.
[35] D.G. Cahill, Rev. Sci. Instrum. 61 (2) (1990) 802.
[36] D.G. Cahill, et al., Phys. Rev. B 50 (9) (1994) 6077.
[37] D. De Koninck, Thermal Conductivity Measurements Using the 3-omega Technique: Application to Power Harvesting Microsystems, McGill University, 2008.
[38] J.P. Feser, Scalable Routes to Efficient Thermoelectric Materials, University of California, Berkeley, 2010.
[39] W.-Y. Lee, et al., J. Nanoelectron. Optoelectron. 12 (9) (2017) 986.
[40] H.J. Goldsmid, Thermoelectric Refrigeration, Plenum, New York, 1964.
[41] J. de Boor, E. Müller, Rev. Sci. Instrum. 84 (6) (2013) 065102.
[42] J.H. Kim, et al., J. Appl. Phys. 86 (7) (1999) 3959.
[43] H.-C. Chien, et al., Rev. Sci. Instrum. 79 (5) (2008) 054902.
[44] X. Wang, B. Huang, Sci. Rep. (2014) 4.
[45] G. Chen, Nanoscale Energy Transport and Conversion: a Parallel Treatment of Electrons, Molecules, Phonons, and Photons, Oxford University Press, New York, 2005.
[46] T. Zeng, G. Chen, J. Heat Tran. 123 (2) (2001) 340.
[47] Q. Hao, J. Appl. Phys. 116 (3) (2014) 034305.
[48] K. Esfarjani, et al., Phys. Rev. B 84 (8) (2011) 085204.
[49] A. Majumdar, J. Heat Tran. 115 (1) (1993) 7.
[50] G.S. Springer, Heat transfer in rarefied gases, in: Advances in Heat Transfer, vol. 7, Elsevier, 1971, p. 163.
[51] D.P. Sellan, et al., J. Appl. Phys. 108 (11) (2010) 113524.
[52] J. Ordonez-Miranda, et al., J. Appl. Phys. 118 (7) (2015) 075103.
[53] Y. Hu, et al., Nat. Nanotechnol. 10 (8) (2015) 701.
[54] Z. Tian, et al., Appl. Phys. Lett. 99 (5) (2011) 141.
[55] D. Li, et al., Appl. Phys. Lett. 83 (14) (2015) 2934.
[56] Q. Hao, et al., Sci. Rep. 8 (1) (2018) 9056.
[57] C. Jeong, et al., J. Appl. Phys. 111 (9) (2012) 093708.
[58] P.E. Hopkins, et al., Nano Lett. 11 (1) (2011) 107.
[59] A. Jain, et al., Phys. Rev. B 87 (19) (2013) 195301.
[60] A. Ward, D. Broido, Phys. Rev. B 81 (8) (2010) 085205.
[61] L.J. Porter, et al., J. Appl. Phys. 82 (11) (1997) 5378.
[62] W.T. Read, W. Shockley, Phys. Rev. 78 (3) (1950) 275.
[63] A. Otsuki, Interface Sci. 9 (3–4) (2001) 293.
[64] Q. Meng, et al., Phys. Rev. B 87 (6) (2013) 064102.
[65] C.A. Polanco, et al., Phys. Rev. B 95 (19) (2017) 195303.
[66] X. Ji, et al., J. Appl. Phys. 104 (3) (2008) 034907.
[67] T.S. English, et al., Phys. Rev. B 85 (3) (2012) 035438.
[68] S.I. Kim, et al., Science 348 (6230) (2015) 109.